

# Adaptation of the base-paired double-helix molecular architecture to extreme pressure

Eric Girard<sup>1,\*</sup>, Thierry Prangé<sup>2</sup>, Anne-Claire Dhaussy<sup>3</sup>, Evelyne Migianu-Griffoni<sup>4</sup>, Marc Lecouvey<sup>4</sup>, Jean-Claude Chervin<sup>5</sup>, Mohamed Mezouar<sup>6</sup>, Richard Kahn<sup>7</sup> and Roger Fourme<sup>1</sup>

<sup>1</sup>Synchrotron-SOLEIL, L'Orme des Merisiers, Saint-Aubin, BP 48, 91192 Gif-sur-Yvette Cedex, <sup>2</sup>Laboratoire de Cristallographie et RMN Biologiques (UMR 8015 CNRS) Université Paris-5, 4 Avenue de l'Observatoire, 75006 Paris, <sup>3</sup>CRISMAT, ENSICAEN, Boulevard du Maréchal Juin, 14000 Caen, <sup>4</sup>BioMoCeTi (UMR CNRS 7033), UFR S.M.B.H., Université Paris-13, 74 rue Marcel Cachin, 93017 Bobigny Cedex, <sup>5</sup>PMD, IMPMC, Université Pierre et Marie Curie – CNRS UMR7590, 140 rue de Lourmel, 75015 Paris, <sup>6</sup>ESRF, BP 220, 38027 Grenoble Cedex and <sup>7</sup>IBS, UMR 5075 CEA-CNRS-UJF, 41 rue Jules Horowitz, 38027 Grenoble Cedex, France

Received May 3, 2007; Revised and Accepted June 13, 2007

## ABSTRACT

**The behaviour of the d(GGTATACC) oligonucleotide has been investigated by X-ray crystallography at 295 K in the range from ambient pressure to 2 GPa (~20 000 atm). Four 3D-structures of the A-DNA form (at ambient pressure, 0.55, 1.09 and 1.39 GPa) were refined at 1.60 or 1.65 Å resolution. In addition to the diffraction pattern of the A-form, the broad meridional streaks previously explained by occluded B-DNA octamers within the channels of the crystalline A-form matrix were observed up to at least 2 GPa. This work highlights an important property of nucleic acids, their capability to withstand very high pressures, while keeping in such conditions a nearly invariant geometry of base pairs that store and carry genetic information. The double-helix base-paired architecture behaves as a molecular spring, which makes it especially adapted to very harsh conditions. These features may have contributed to the emergence of a RNA World at prebiotic stage.**

## INTRODUCTION

Nucleic acids are more plausible than proteins as the components of a self-contained replicating system in the very first stages of the emergence of life on Earth (1–3). Watson–Crick base pairing provided a very plausible mechanism by which a polynucleotide could direct the synthesis of its complement from mononucleotides or short oligonucleotides, while no equivalent mechanism is known for the replication of a polypeptide. The discovery

of ribozymes (4,5) and then the demonstration that ribosomal peptide synthesis is a ribozyme-catalysed reaction (6) strengthened the case for an early RNA World. In this context, the central problem for origin-of-life studies is to understand how this seminal world became established on the primitive Earth. Plausible scenarios for the prebiotic chemistry have been proposed (7,8), but the problem is far from being solved. A recurrent theme is that RNA may have emerged from an earlier world under extreme conditions of pressure and/or temperature and pH (8). In all scenarios, molecules with backbones forming stable double helices held together by Watson–Crick base pairing appear as crucial intermediates or crucial building blocks. This fact led us to undertake a programme on the behaviour of such molecules under high pressure.

Some studies were recently devoted to the analysis of the effects of high hydrostatic pressures on the stability of living cells (9–11), the quaternary structures of proteins and viruses (12), protein–protein and protein–DNA interactions (13), catalytic RNA (14) and tRNA (15). Concerning nucleic acids, they were investigated through their single-strand/duplex equilibrium (16), their B/Z transition (17) and their hydration networks (18) all using spectroscopic techniques in solution. Following Le Chatelier's principle, pressure tends to favour states with smaller specific volumes. In DNA, structural adaptation to high pressure results from several contributions, including the helical structure integrity (helix-to-coil transition), the stacking of bases, the Watson–Crick association and the hydration network around the duplex. Aromatic-ring stacking is favoured by pressure while Coulombic or hydrophobic interactions are

\*To whom correspondence should be addressed. Tel: +33 169359609; Fax: +33 169359456; Email: eric.girard@synchrotron-soleil.fr

The authors wish it to be known that, in their opinion, the first two authors should be regarded as joint First Authors.

© 2007 The Author(s)

This is an Open Access article distributed under the terms of the Creative Commons Attribution Non-Commercial License (<http://creativecommons.org/licenses/by-nc/2.0/uk/>) which permits unrestricted non-commercial use, distribution, and reproduction in any medium, provided the original work is properly cited.

disfavoured (19). Hydrogen bonds and associated networks should be, as in protein and protein assemblies (20–22), stabilized by pressure. How these various parameters influence the structure and stability of the DNA duplex is not easy to predict. Clearly, besides spectroscopic data, accurate 3D structures were required in order to describe the behaviour under high pressure at the molecular level and provide a firm starting point for simulations. With respect to pioneering work based on high-pressure beryllium cell (23), our technical developments combining diamond anvil cell and synchrotron radiation of ultrashort wavelength (24) have considerably extended the possibilities of high-pressure macromolecular crystallography (HPMX) in a pressure range increased by one order of magnitude (from 0.2 to 2 GPa). After studies on monomeric (20), then multimeric (25) proteins and a complex protein assembly (21), this article reports the first application of HPMX to nucleic acids.

The d(GGTATACC) oligonucleotide was selected owing to the high stability of its crystalline A-DNA crystalline form, its strong base stacking (2.9 Å compared to the 3.3 Å in B-DNA duplex), and its particularly well-defined hydrogen-bonding network, mostly located in the major groove (26). The last reason for this choice is an interesting feature related to the crystal packing of d(GGTATACC) crystals. Besides Bragg reflections of the A-form crystal, a pattern was observed on diffraction pictures of nucleotide crystals, similar to fibre diagrams that led Watson and Crick to their interpretation of the DNA structure (27). Main features of this pattern include a characteristic diffuse crossed X-ray pattern, a set of streaks perpendicular to the  $c^*$  direction of the reciprocal lattice and two strong elongated meridian reflections (28). The following interpretation for the origin of this pattern was proposed (28). Oligonucleotide molecules pack in infinite super-helices of duplexes down the 6-fold axis of the  $P6_1$  space group (26). The central channel of the super-helix can trap oriented molecules of DNA. Simulations of streaks allow excluding the A-form for occluded molecules and favour the B-form. The meridional reflections are consistent with the base-pair stacking in B-form molecules. According to these results, we have in hand a system in which both A and B forms of DNA can be simultaneously monitored against external hydrostatic pressure, although information derived on the B-form is obviously quite limited.

Crystals of the nucleotide were compressed up to 2 GPa at 295 K. We describe the high-resolution crystal structures of A-DNA at four pressures from ambient to 1.39 GPa. Meridional streaks attributed to B-DNA are observed up to at least 2 GPa. These results highlight the remarkable adaptation of the base-paired double-helix architecture base-paired architecture to high pressure.

## MATERIALS AND METHODS

### Preparation and crystallization

The d(GGTATACC) sequence was synthesized by standard phosphoramidite chemistry on solid support (Applied Biosystems 391 DNA Synthesizer). Crystals

were obtained following the batch method (26). Ten milligrams of lyophilized octamer were dissolved in 200  $\mu$ l of a 15% methyl-pentane-diol (MPD) solution, buffered by sodium cacodylate ( $5 \times 10^{-2}$  M, pH 7) and containing additives: sodium azide, spermine tetrahydrochloride and  $MgCl_2$ . To this solution, was added each day 5  $\mu$ l of the same solution but containing 50% of MPD, followed by a rapid mixing. After 5 days, crystals began to appear as elongated hexagonal rods and grew easily to a size of  $0.2 \times 0.2 \times 1.0$  mm<sup>3</sup> in a week. They were stabilized by increasing the final MPD concentration to  $\sim 35\%$ .

### High-pressure cell

Crystals were hydrostatically compressed in a diamond anvil cell. The compression chamber (diameter 400  $\mu$ m, height 200  $\mu$ m) was drilled in a copper or stainless steel (for pressure above 0.7 GPa) gasket (Figure 1). Gasket preparation and sample loading were performed as described (24). The crystallization solution with 35% MPD was used as compression medium. Pressure monitoring was performed by using the wavelength shift of laser-excited fluorescence from a small ruby sphere loaded in the compression chamber. Two different diamond anvil cells were used for data collection. The first one had a useful aperture of 62° and a standard diamond mount (24). The second one was of a novel design to provide both a larger useful aperture (82°) and a pressure range up to  $\sim 2.5$  GPa (29).

### Data collection

Diffraction data from crystals compressed in the diamond anvil cell were collected at the ESRF (Grenoble, France), on the ID27 beamline with a MAR CCD 165 mm detector. The wavelength was calibrated and set to 0.3738 Å (Iodine K absorption edge). Four data sets were collected at room temperature and ambient pressure, 0.55, 1.04 and 1.39 GPa. The crystal-to-detector distance,

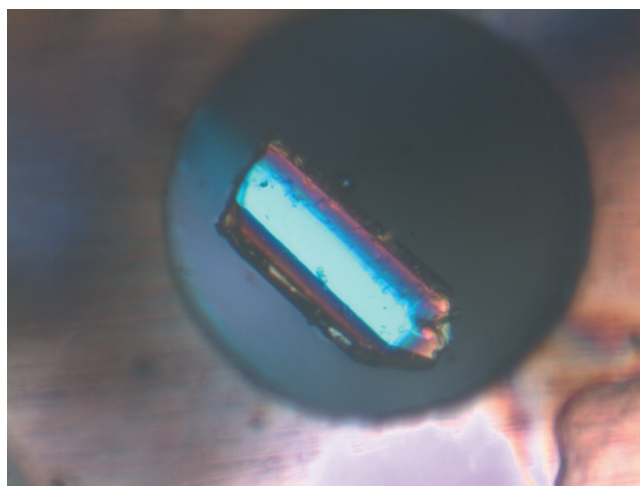


**Figure 1.** A d(GGTATACC) crystal inside the compression chamber ready for pressurization, observed through the diamond anvils. The diameter of the chamber, drilled by electro-erosion into a copper foil, is 400  $\mu$ m and the depth is 200  $\mu$ m.

calibrated using the diffraction rings of a reference silicon powder, was 352.9 mm for the 0.55 GPa data set and 302.9 mm for the others. The X-ray beam was collimated to  $50 \times 50 \mu\text{m}^2$ . Exposure times were 30 or 45 s, depending on the sample, for a rotation step of  $1^\circ$ . As data collection was performed at room temperature, crystals were translated several times, every 10 to  $35^\circ$  of rotation, during exposure in order to irradiate fresh zones (24).

### Data processing

Diffraction frames were integrated using XDS (30). All data were independently put on an absolute scale using SCALA (31).

### Refinement

The starting molecular model was either the deposited coordinates ref. 115D (26) or 1VJ4 (32) from the Protein Data Bank. In the case of 115D, the isomorphous di-bromo derivative of 1VJ4, thymine residues were reconstructed from original bromo-uracils and all water molecules were removed. A first round of rigid body refinements was done with AMoRe (33), then refinements proceeded at the maximum resolution with individual isotropic thermal factors and bond distance and angle restraints, as used in SHELXL (34). Water molecules were localized during the course of refinement cycles by analyzing density peaks in  $F_o - F_c$  Fourier difference maps. They were accepted when they met standard criterions like correct bond distances and angles toward polar atoms of the model, and B thermal factors below a given threshold arbitrarily fixed to  $65 \text{ \AA}^2$ . All analyses of the geometric parameters were done using NEWHEL93 (35). All molecular figures were created using the program PyMol (<http://pymol.sourceforge.net/>).

## RESULTS AND DISCUSSION

Single crystals of d(GGTATACC) were gradually compressed from atmospheric pressure to 2 GPa (Figure 1). Unit cell parameters of the A-DNA crystal were measured at each step of the pressure ramp from diffraction data recorded over a rotation range of  $2^\circ$ . In spite of the elongated (anisotropic) shape of the DNA cylinder, they decrease isotropically up to a pressure value of  $\sim 1.5$  GPa. The isothermal compressibility of the crystal is defined as  $\chi = -1/V(\partial V/\partial P)_T$ , where  $V$  is the unit-cell volume. The variation of  $V$  is shown in Figure 2. Least-squares fit up to 1.5 GPa is  $V(P) = V(\infty) + k_1 \exp(-k_2 \cdot P)$  with  $V(\infty) = 62290 \text{ \AA}^3$ ,  $k_1 = 11030 \text{ \AA}^3$  and  $k_2 = 1.25 \text{ GPa}^{-1}$ . The derived isothermal compressibility is  $\chi(P) = V^{-1} \cdot k_1 \cdot k_2 \cdot \exp(-k_2 \cdot P)$ . The largest value is at ambient pressure ( $\chi_0 = 0.215 \text{ GPa}^{-1}$ ). We recall that the compressibility of bulk water is  $0.35 \text{ GPa}^{-1}$ ; the compressibility of water in the vicinity of polar atoms is similar to that of an 'ice-like' structure,  $0.18 \text{ GPa}^{-1}$  (36). The mean value of  $\chi(P)$  between ambient pressure and 1.5 GPa is  $0.088 \text{ GPa}^{-1}$ , similar to the compressibility of tetragonal hen egg-white lysozyme crystal (23,24). Above  $\sim 1.6$  GPa, the cell volume increases (the compressibility is negative) and the crystal quality, as monitored by mosaicity and resolution of

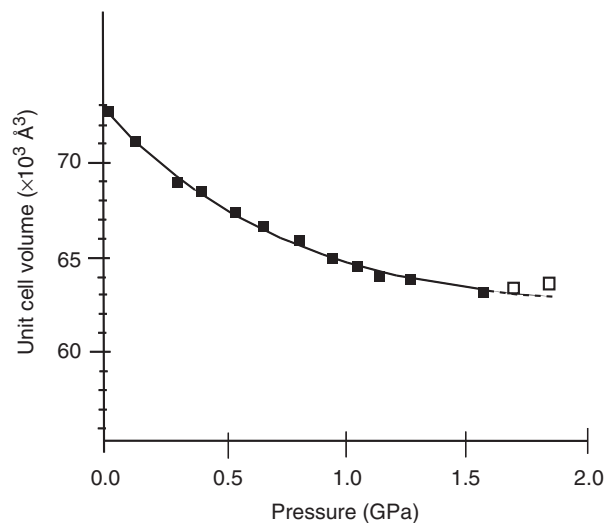


**Figure 2.** A-DNA pressure variation at 295 K of crystal unit-cell volume  $V$  versus pressure (rmsd's on cell dimensions and pressures are estimated as  $2 \times 10^{-3} \text{ \AA}$  and  $10^{-2} \text{ GPa}$ , respectively).

diffraction data, gradually deteriorates. The diffraction that extends to  $1.6 \text{ \AA}$  at ambient pressure falls off to  $3 \text{ \AA}$  at  $\sim 1.8$  GPa and is completely lost at  $\sim 2.0$  GPa. Four high-resolution structures of the A-DNA form were determined at ambient pressure, 0.55, 1.04 and 1.39 GPa. In each case, one or two crystals were sufficient to acquire high-completeness data (Table 1) in spite of data collection at room temperature. Refinements were performed at  $1.60\text{--}1.65 \text{ \AA}$  resolution to R-factors (R-free factors) of 15.2 (19.1), 16.9 (20.1), 19.3 (22.7) and 18.8 (22.6)%, respectively (Table 2).

The overall duplex structures shown in Figure 3 evidence axial compression of the helix, which reacts to pressure like a molecular spring. The base-stacking shrinkage is  $2.6 \text{ \AA}$  for the full octamer length (from  $23.5 \text{ \AA}$  at ambient pressure to  $20.9 \text{ \AA}$  at 1.39 GPa, i.e. a relative contraction of 11%). The average base-pair step varies from  $2.92 \text{ \AA}$  down to  $2.73 \text{ \AA}$  (Figure 4). This spectacular plasticity associates only small changes in phosphodiester backbone angles for accounting the denser base stacking. The sugar puckering parameters (Taum and P) describing the sugar conformations were analysed. All of them belong to the canonical C3'endo (or northern) conformation, a behaviour already mentioned earlier (26). The pseudo-rotation P remains remarkably constant over the whole pressure range between standard values of  $1$  to  $30^\circ$ , including the O3' end sugar of chain A, which moves from  $30.9$  to  $33.3^\circ$ . The only exception is the O3' end sugar of chain B that adopts at ambient pressure a C2'/C1' twist (nearly a southern conformation) and goes back to  $36.8^\circ$  (northern) at 1.04 GPa and above.

The variation of base-pair spacing versus pressure (Figure 4) is approximately linear up to 1.0 GPa and becomes steady beyond, which means that the molecule becomes progressively unable to accommodate increasing compression. The gradual degradation of the crystal order beyond  $\sim 1.6$  GPa may be due, at least partly, to this effect.

**Table 1.** Statistics of data collection at 295 K for the four d(GGTATACC) crystal structures. The space group is P6<sub>1</sub>. X-ray wavelength was 0.3738 Å

Pressure (GPa)	Ambient	0.55	1.04	1.39
Cell parameters (Å), (esd's = 0.002 Å)	<i>a</i> = <i>b</i> = 45.034 <i>c</i> = 41.747	<i>a</i> = <i>b</i> = 43.710 <i>c</i> = 40.710	<i>a</i> = <i>b</i> = 43.171 <i>c</i> = 40.383	<i>a</i> = <i>b</i> = 42.830 <i>c</i> = 40.300
Resolution range (Å)	19–1.60	18–1.65	18–1.60	18–1.60
Number of crystals used	2	1	1	1
Number of measured reflections	24 124	16 086	16 460	17 039
Number of unique reflections	6 015	5 038	5 079	5518
<i>R</i> <sub>merge</sub> (%)	4.7 (33.0)	4.3 (18.8)	5.8 (25.1)	4.7 (33.1)
<i>I</i> / $\sigma$ ( <i>I</i> )	9.3 (2.3)	10.2 (3.9)	6.6 (2.9)	11.4 (2.2)
Completeness (%)	94.5 (96.2)	94.1 (94.1)	89.4 (91.0)	98.5 (99.3)
Redundancy	4.0 (4.0)	3.2 (2.6)	3.2 (3.3)	3.1 (3.1)

Last resolution shell in parentheses.

**Table 2.** Refinement statistics

Pressure (GPa)	Ambient	0.55	1.04	1.39
Number of atoms in the model	322	322	322	322
Number of water molecules	57	75	75	76
Number of additional atoms (spermine)	–	–	10	10
R factor (on observed F)%	14.86	16.93	18.92	18.66
R factor (all F data)%	15.85	18.64	20.15	20.07
R-free factor (8% of F data)%	18.9	20.1	22.1	22.2
wR2 factor (all F <sup>2</sup> data)%	39.2	43.2	46.2	47.8
Number of parameters/No. restraints	1523/1585	1595/1594	1651/1653	1691/1729
Solvent fraction in the unit cell (%)	49.2	44.7	43.6	41.8
Average thermal parameters (Å <sup>2</sup> ) (Number of atoms in parentheses)				
Base planes (152)	16.5	18.4	16.4	22.0
Sugars (96)	19.0	22.6	20.8	27.4
Phosphate chains (74)	24.3	30.5	27.6	32.3
All water molecules	44.9	47.0	40.8	39.6
Common water molecules (46)*	40.6	37.1	34.6	34.1
1st shell water molecules	45.2	46.3	40.2	38.3
2nd shell water molecules	43.1	47.5	41.7	40.7
Deviations from ideal values (Number of restraints in parentheses)				
Bond distances (1–2 dist) (Å)	0.012 (392)	0.010 (392)	0.009 (405)	0.009 (406)
Bond angles (1–3 dist) (°)	0.039 (656)	0.028 (656)	0.027 (668)	0.030 (684)
Planarity (Å)	0.014 (120)	0.016 (120)	0.015 (120)	0.021 (120)
Non-zero chiral volumes (Å <sup>3</sup> )	0.007 (48)	0.007 (48)	0.007 (48)	0.008 (52)
Last difference-Fourier map min/max (e-/Å <sup>3</sup> )	–0.23/+0.30	–0.23/+0.33	–0.29/+0.39	–0.26/+0.30

\*Water molecules observed in common sites for all structures.

Contrary to common B-DNA crystal packing arrangements, where duplexes stack on the top of each others building infinite helices along crystal axes, the hexagonal packing of d(GGTATACC) builds infinite super-helices around the 6-fold crystallographic axis with a close-contact zone between neighbouring helices (26,28). In this region, the wedge effect of hydrostatic pressure produces a hinge point in base stacking between the fifth and the sixth base pairs (Figure 5). This steric effect might also contribute to crystal degradation.

The Watson–Crick type of base-pair association, which represents the foundation of the genetic code transmission, could be another way for the helix to ‘breathe’ transversally. In proteins, in the elastic compression regime, salt bridges and H-bond lengths are usually shortened by  $\sim 0.1 \text{ \AA} \cdot \text{GPa}^{-1}$  (20–22). In the case of A-DNA, evolutions of polar atom distances within G–C and A–T base pairs (Table 3) can be interpreted in terms

of small variations of rise, buckle, propeller-twist and other parameters that contribute to the adaptation to high pressure (Table 4). Accordingly, the geometry of Watson–Crick base pairings remains essentially invariant in the pressure domain up to 1.39 GPa. The lengths of vectors C1'–C1', that may be used to quantify the DNA cylinder transversal squeeze, are all identical within their SDs, i.e. 10.5(2) Å, whatever the applied pressure.

It was suggested from modelling and docking simulations that water hydration under high hydrostatic pressure would tend to build octahedral arrangements (17) around DNA, to account for a negative  $\Delta V$ . These arrangements have been invoked in the B/Z transition observed under high pressure (15). The A-form of DNA shows a heavily hydrated major groove and a poorly hydrated minor groove. These features are distinct with respect to other DNA forms, and as such are worth to be investigated under pressure. The hydration scheme of d(GGTATACC)

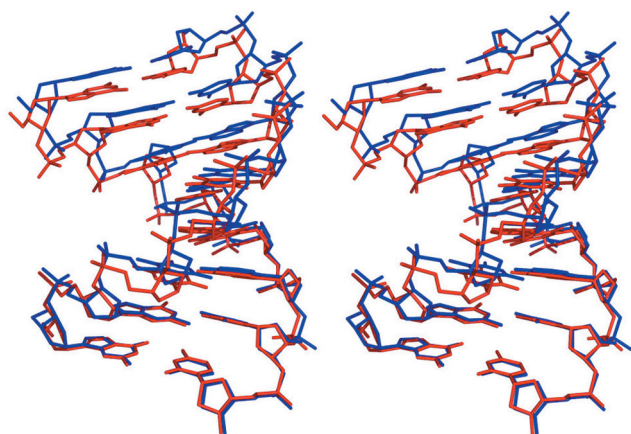


**Figure 3.** Stereo superimposition of the A-DNA duplex at ambient pressure (blue) and 1.39 GPa (red). The full duplex length reduces from 23.5 Å at ambient pressure to 20.9 Å at 1.39 GPa. Bound water molecules are omitted. Superimposition was made by fitting the C8(a)–G1(b) base pair.

has been extensively analysed because it presents regular pentagonal arrangements (26) in the major groove (Figure 6), a typical motif also observed in some well-ordered proteins at atomic resolution such as crambin (37). The particular conformation of the A-form of DNA allows water molecules to directly bridge phosphate groups along each individual strand. At ambient pressure, 75 direct polar contacts are established through 51 water molecules belonging to the first shell of hydration, including nine over the 12 possible phosphate bridges. As mentioned earlier, the remaining water molecules build an ordered network from rim to rim thus completely filling most of the available space in the major groove. Under pressure, more water sites become apparent. This is illustrated in Figure 7, which shows the same G–C base pair at one end of the duplex superimposed to the  $2F_o - F_c$  electron-density maps calculated at different pressures. At 0.55 GPa, the number of observed isolated peaks in the first shell of hydration increases to 69, although some of them were suspected not to correspond to water sites as they fill parts of elongated electron densities that cannot be connected to the model. When pressure is increased above 1.04 GPa, one of the elongated densities resolves as a linear chain, ideally fitting a folded spermine molecule. The stabilization of the hydrogen-bond network is made evident by a slow but continuous decrease of the average normalized  $\langle B_i \rangle$  thermal factor of water molecules common to all structures (Table 2) down to a limit of  $\sim 34 \text{ \AA}^2$ . The number of direct polar contacts from the first shell of hydration to the oligomer also increases rapidly with pressure up to 0.55 GPa, then more slowly up to 1.39 GPa. Beyond 1 GPa, the first shell of hydration is gradually compressed thus leading to more direct contacts towards the DNA (Table 2). Nevertheless, the pentagonal network located in the major groove remains conserved in the whole pressure range.

The four X-ray data sets were recorded with exposure times appropriate for collecting the A-form diffraction data but too short to get a complete picture of the diffuse

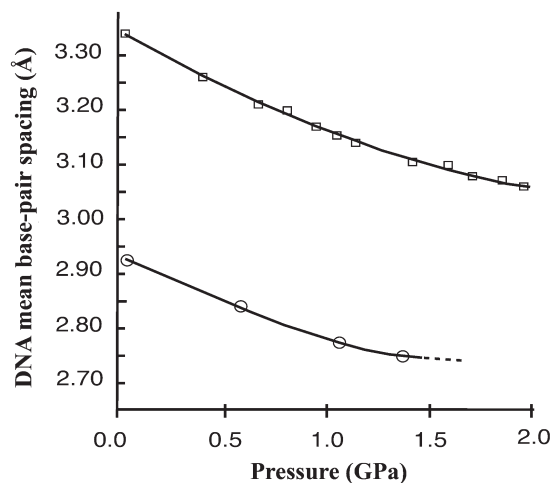


**Figure 4.** Average base-pair spacing dependencies upon increasing hydrostatic pressure. Open circles: crystalline A-DNA form; results derived from the four refined crystal structures. Open squares: B-DNA in liquid environment; results derived from meridional reflections in the fibre diagram produced by molecules occluded in channels of the A-form packing.

scattering pattern described in (28). The series of narrow streaks distributed in the pattern of a cross was barely observable, but the extended meridional streaks associated with the base-pair stacking were clearly observed up to at least 2 GPa. According to the interpretation given in (28), the diffuse scattering pattern is produced by occluded B-DNA molecules in the packing channels of the A-DNA crystal structure. A suitable orientation of crystals in the high-pressure cell allowed us to record these meridional streaks (Figure 8) while ramping pressure, which provided data to determine the average stacking distance. A continuous and smooth shortening is observed, that can be monitored even in the range 1.5–2 GPa where the A-DNA crystal order falls off (Figure 4). The average base-pair step is 3.34 Å at ambient pressure and 3.07 Å at 2 GPa.

## CONCLUSION

We have shown that d(GGTATACC) in the crystalline A-form can withstand very high pressures, up to  $\sim 1.9$  GPa. The gradual loss of long-range order between 1.6 and 1.9 GPa may be related partially or completely to packing effects as mentioned previously and the molecule in solution might be stable even beyond 1.9 GPa. The four high-resolution structures show that geometry of base pairs is well preserved under compression up to at least 1.39 GPa. The B-form molecules occluded in channels of the crystal packing are in a solution-like environment. The information derived on this form from diffuse scattering is limited. Nevertheless, the smooth variation of the period of stacking derived from the evolution of meridian streaks reveals that the B-form is probably stable up to at least 2 GPa. We shall consolidate and extend this preliminary result by performing another single-crystal study on a dodecanucleotide that crystallizes in the B-DNA form.

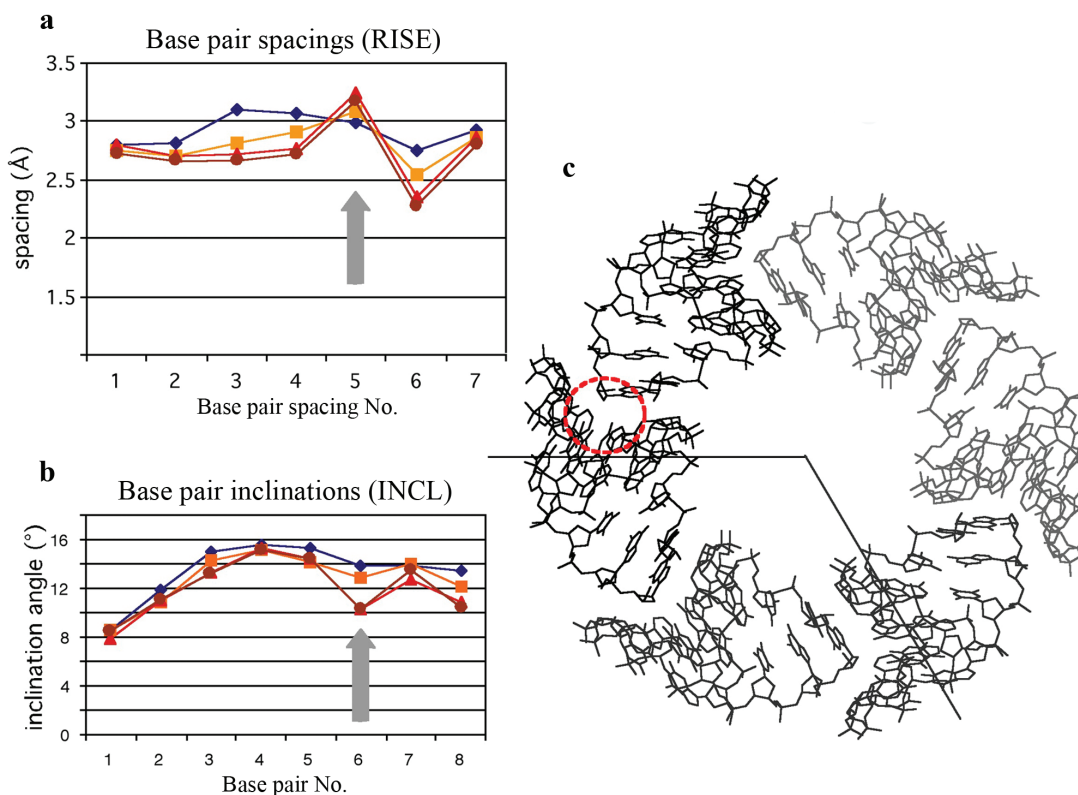


**Figure 5.** Evolution of base-pair parameters (35) as a function of applied hydrostatic pressure. (a) the RISE and (b) the INCL values at ambient pressure (blue), 0.55 GPa (yellow), 1.04 GPa (red) and 1.39 GPa (green). In each diagram, the arrow points towards the position where another duplex molecule induces in the crystal packing a hinge effect as shown in (c) (open red circle).

**Table 3.** Main helical parameters in d(GGTATACC) (errors on distances estimated as  $\pm 0.035$  Å, based on refined coordinates). Temperature is 295 K

Pressure (GPa)	Ambient	0.55	1.04	1.39
Watson-Crick distances (Å)				
G-C base pairs				
O6-N4	2.90	2.95	2.96	2.90
N1-N3	2.92	2.88	2.89	2.83
N2-O2	2.84	2.80	2.81	2.76
A-T base pairs				
N1-N3	2.86	2.82	2.81	2.74
N6-O4	2.97	2.90	2.99	2.98
Total number of water molecules located	57	75	75	76
Number of water molecules in the 1 <sup>st</sup> sphere of hydration ( $d < 3.4$ Å)	51	69	65	71
Number of polar contacts to the 1 <sup>st</sup> sphere of hydration	75	94	103	115
Distances (Å) in range				
2.00-2.40	2	7	5	7
2.40-2.80	20	27	29	32
2.80-3.20	37	44	40	46
3.20-3.40	16	16	29	30
Common water molecules				
Average bond distance (Å)	2.95	2.91	2.95	2.94
Average isotropic thermal factor B (Å <sup>2</sup> )	40.6	37.1	34.6	34.1

For all pressures, base-plane atoms (152), sugar atoms (96) and phosphate atoms (74) have their  $\langle B \rangle$  parameters in the ranges,  $[16-20 \text{ Å}^2]$ ,  $[18-26 \text{ Å}^2]$  and  $[22-32 \text{ Å}^2]$ , respectively.

The remarkable adaptation of d(GGTATACC) to high pressure is clearly associated to the base-paired double-helix topology of the molecule, by which it behaves as a molecular spring. These properties are probably shared by molecules featuring similar topology, with sugar-phosphate or polypeptide backbones. At the prebiotic stage, the base-paired double-helix architecture was crucial in the emergence of molecules with catalytic properties and able to store genetic information. Such architectures could withstand not only pressure in the deepest sea trenches but also much higher pressures found in Earth's interior or in the context of rare events such as impact of a meteorite. We suggest that this remarkable adaptation to harsh conditions may have played an important role during the sequence of events that led to the seminal RNA World.

## ACKNOWLEDGEMENTS

HPMX data collection was performed in the context of a Long-Term Project (MX421) at the ESRF (Principal Investigator R. Fourme). Funding came from CNRS and CEA. We thank the staff of the ID27 beam line—and especially W. Crichton—for help and advice during experiments, Bernard Couzinet (IMPIC, Paris) for its participation in the design of the wide-aperture diamond anvil cell and Andrea Dessen (IBS, Grenoble) for critical reading of the manuscript. Funding to pay the Open

**Table 4.** Base plane geometry versus external hydrostatic pressure, according to NEWHEL93 (35)

Pressure (GPa)	Step	Rise (Å)	Twist (°)	Roll (°)	Buckle (°)	Propeller (°)	Slide (Å)	Tilt (°)	Inclination (°)
Ambient	1	2.786	33.57	6.42	7.47	-4.89	-3.44	-0.10	8.63
	2	2.817	32.09	-0.08	14.03	-12.11	-2.80	1.63	11.82
	3	3.096	29.93	12.19	6.71	-9.20	-2.55	0.29	14.96
	4	3.078	33.22	2.10	2.02	-11.61	-2.61	0.06	15.64
	5	2.994	31.38	14.86	-7.64	-12.51	-2.85	-0.92	15.32
	6	2.748	31.91	3.84	-7.64	-14.04	-3.01	-0.67	13.81
	7	2.920	31.81	8.05	-8.46	-12.21	-3.24	-0.13	13.86
	8	-	-	-	-8.78	-0.49	-	-	13.36
	Mean	2.92	31.99	6.77	-0.22	-9.63	-2.93	0.02	13.42
0.55	1	2.754	31.95	8.07	3.67	-6.12	-1.81	-0.11	8.57
	2	2.702	36.58	0.18	11.07	-15.21	-1.04	1.69	10.91
	3	2.821	30.00	12.39	3.81	-12.24	-1.26	0.54	14.27
	4	2.913	33.98	-0.04	4.04	-12.01	-0.96	-0.06	15.20
	5	3.091	30.44	18.45	-8.75	-15.14	-1.34	-0.85	14.18
	6	2.538	34.76	1.28	-7.44	-17.45	-1.17	-0.30	12.87
	7	2.867	31.76	9.39	-10.07	-17.50	-1.65	-1.46	13.96
	8	-	-	-	-9.89	-3.09	-	-	12.20
	Mean	2.81	32.78	7.10	-1.69	-12.35	-1.32	-0.08	12.77
1.04	1	2.797	31.73	7.03	6.40	-6.60	-1.83	0.47	7.90
	2	2.696	37.34	1.32	8.42	-14.66	-0.98	0.53	10.99
	3	2.712	29.51	12.25	2.30	-10.26	-1.28	1.04	13.29
	4	2.766	35.21	-0.89	4.54	-13.82	-1.10	-0.22	15.29
	5	3.246	29.58	19.47	-6.95	-15.03	-1.40	-4.04	14.36
	6	2.352	35.94	-0.79	-11.82	-19.16	-1.15	0.28	10.35
	7	2.865	31.52	8.47	-9.38	-19.20	-1.73	-1.80	12.75
	8	-	-	-	-7.74	-1.80	-	-	10.92
	Mean	2.78	32.98	6.70	-1.78	-12.57	-1.35	-0.53	11.98
1.39	1	2.734	31.79	9.22	2.67	-8.01	-1.96	0.28	8.28
	2	2.650	36.44	1.70	7.33	-14.94	-1.02	0.42	10.32
	3	2.672	30.34	12.03	2.90	-11.44	-1.35	1.08	12.57
	4	2.722	35.51	-1.24	4.87	-13.92	-1.16	-0.58	15.36
	5	3.194	29.57	18.88	-6.45	-15.15	-1.39	-3.83	14.20
	6	2.302	36.2	-1.86	-11.53	-18.24	-1.12	0.60	10.46
	7	2.837	32.18	9.80	-11.34	-20.36	-1.72	-1.27	12.45
	8	-	-	-	-6.39	-2.31	-	-	10.54
	Mean	2.77	33.15	6.93	-2.24	-13.05	-1.39	-0.47	11.77

Some parameters describing the geometry, in particular RISE and TWIST parameters, are very sensitive to packing hinge effect of one helix over the preceding one in the super-helix built along the *c* axis as shown in the diagrams in Figure 5.

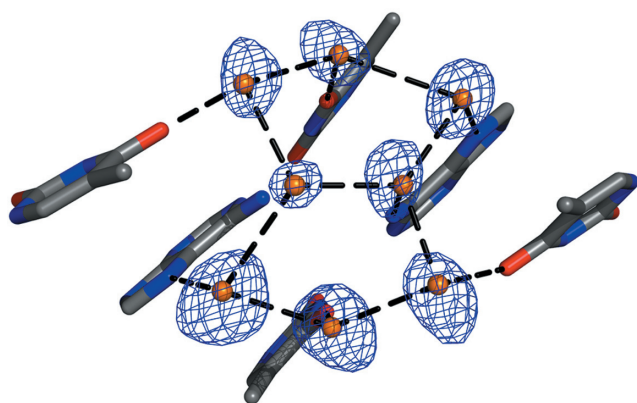


**Figure 6.** The two pentagons of water molecules located in the major groove. They are visible in the whole pressure range. The  $(2F_o - F_c)$  density map is contoured at  $1\sigma$  above the average background. Hydrogen bond with distances  $<3.2\text{Å}$  are indicated with dashed lines.

Access publication charges for this article were provided by CNRS and CEA laboratories.

**Author Contributions.** E.G., T.P. and R.F. designed the project. E.M.-G. and M.L. synthesized the

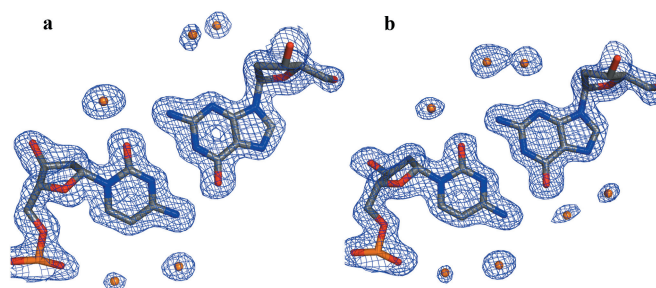


**Figure 7.** Two views of the same Watson-Crick base pair G1(a)-C8(b) electron density, located at one end of the duplex (a, ambient pressure; b, 1.39 GPa) show the progressive appearance of water molecules (single globular densities). Electron-density maps are calculated with refined phases and contoured at  $1\sigma$  above the average background.

d(GGTATACC) sequence. J.-C.C. designed the wide-aperture diamond anvil cell. E.G., T.P., A.-C.D., M.M. and R.K. performed the experiments. E.G., T.P. and R.K. analysed the diffraction data, ran the refinements and wrote the article together with R.F.

**Accession codes.** Final coordinates and structure factor amplitudes for the structures at ambient pressure, 0.55,

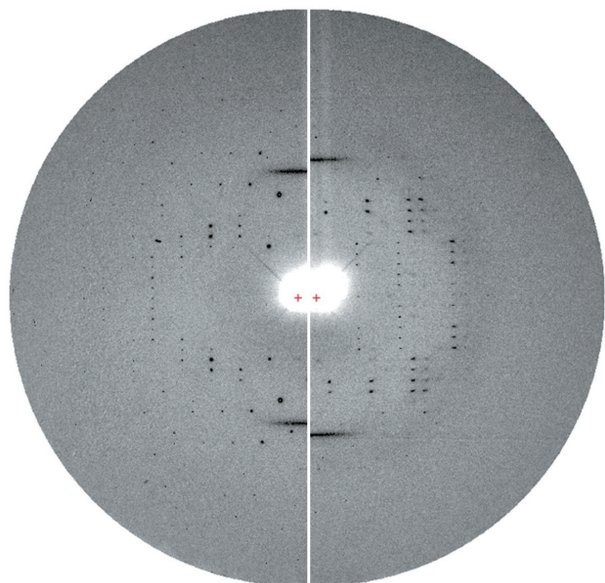


**Figure 8.** Diffuse scattering of B-DNA superimposed to the diffraction pattern of A-DNA crystal at ambient pressure (left) and 1.83 GPa (right). At 1.83 GPa, the two B-DNA meridional reflections still persist over the degrading A-DNA diffraction pattern.

1.09 and 1.39 GPa, respectively are deposited with the Protein Data Bank (accession codes 2PKV, 2PL4, 2PL8 and 2PLB).

*Conflict of interest statement.* None declared.

## REFERENCES

1. Woese, C. (1967) In *The Genetic Code, the Molecular Basis for Genetic Expression*. Harper and Row, New York.
2. Crick, F.H.C. (1968) The origin of the genetic code. *J. Mol. Biol.*, **38**, 367–379.
3. Orgel, L.E. (1968) Evolution of the genetic apparatus. *J. Mol. Biol.*, **38**, 381–393.
4. Kruger, K., Grabowski, P.J., Zaug, A.J., Sands, J., Gottschling, D.E. and Cech, T.R. (1982) Self splicing RNA: autoexcision and autocyclization of the ribosomal RNA intervening sequence of Tetrahymena. *Cell*, **31**, 147–157.
5. Guerrier-Takada, C., Gardiner, K., Marsh, T., Pace, N. and Altman, S. (1983) The RNA moiety of ribonuclease P is the catalytic subunit of the enzyme. *Cell*, **35**, 849–857.
6. Steitz, T.A. and Moore, P.B. (2003) RNA, the first macromolecular catalyst: the ribosome is a ribozyme. *Trends Biochem. Sci.*, **28**, 411–418.
7. Joyce, G.F. and Orgel, L.E. (1990) Prospects for understanding the origin of the RNA World. In Gesteland, R.F. and Atkins, J.F. (eds), *The RNA World*, 2nd edn. Cold Spring Harbor monograph, NY, pp. 49–77.
8. Orgel, L.E. (2004) Prebiotic chemistry and the origin of the RNA world. *Critical Rev. Biochem. Mol. Biol.*, **39**, 99–123.
9. Mentre, P. and Hui Bon Hoa, G. (2001) Effects of high hydrostatic pressure on living cells: a consequence of the properties of macromolecules and macromolecule-associated water. *Int. Rev. Cytol.*, **201**, 1–84.
10. Sharma, A., Scott, J.H., Cody, G.D., Fogel, M.L., Hazen, R.M., Hemley, R.J. and Huntress, W.T. (2002) Microbial activity at Gigapascal pressures. *Science*, **295**, 1514–1516.
11. Mañas, P. and Mackey, B.M. (2004) Morphological and physiological changes induced by high hydrostatic pressure in exponential- and stationary-phase cells of *Escherichia coli*: Relationship with cell death. *Appl. Env. Microbiol.*, **70**, 1545–1554.
12. Silva, J.L., Oliveira, A.C., Gomes, A.M., Lima, L.M., Mohana-Borges, R., Pacheco, A.B. and Foguel, D. (2002) Pressure induces folding intermediates that are crucial for protein-DNA recognition and virus assembly. *Biochim. Biophys. Acta*, **1595**, 250–265.
13. Chilukuri, L.N., Bartlett, D.H. and Fortes, P.A.G. (2002) Comparison of high pressure-induced dissociation of single-stranded DNA-binding protein (SSB) from high pressure-sensitive and high pressure-adapted marine *Shewanella* species. *Extremophiles*, **6**, 377–383.
14. Hervé, G., Tobé, S., Heams, T., Vergne, J. and Maurel, M.C. (2006) Hydrostatic and osmotic pressure study of the hairpin ribozyme. *Biochim. Biophys. Acta*, **1764**, 573–577.
15. Giel-Pietraszuk, M. and Barciszewski, J. (2005) A nature of conformational changes of yeast tRNA<sup>Phe</sup> high hydrostatic pressure effects. *Int. J. Biol. Macromol.*, **37**, 109–114.
16. Krzyzaniak, A., Furste, J., Erdmann, V., Salanski, P., Jurczak, J. and Barciszewski, J. (1996) High pressure effects on conformation of homo- and heteroduplexes of nucleic acids. *Biochimie*, **78**, 862–867.
17. Barciszewski, J., Jurczak, J., Porowski, S., Specht, T. and Erdmann, V.A. (1999) The role of water structure in conformational changes of nucleic acids in ambient and high-pressure conditions. *Eur. J. Biochem.*, **260**, 293–307.
18. Macgregor, R.B.Jr (2002) The interactions of nucleic acids at elevated hydrostatic pressure. *Biochim. Biophys. Acta*, **1595**, 266–276.
19. Mozhaev, V.V., Heremans, K., Frank, J., Masson, P. and Balny, C. (1996) High pressure effects on protein structure and function. *Proteins*, **24**, 81–91.
20. Fourme, R., Ascone, I., Kahn, R., Girard, E., Mezouar, M., Lin, T. and Johnson, J.E. (2003) New trends in macromolecular crystallography at high hydrostatic pressure. In Winter, R. (ed), *Advances in High Pressure Science and Technology II*, Springer, Heidelberg, pp. 161–170.
21. Girard, E., Kahn, R., Mezouar, M., Dhaussy, A.-C., Lin, T., Johnson, J.E. and Fourme, R. (2005) The first crystal structure of a macromolecular assembly under high pressure: CpMV at 330 MPa. *Biophys. J.*, **88**, 3562–3571.
22. Li, H., Yamada, H. and Akasaka, K. (1998) *Biochemistry*, **37**, 1167–1173.
23. Kundrot, C. E. and Richards, F. M. (1987) Crystal structure of Hen Egg-white lysozyme at a hydrostatic pressure of 1000 atmospheres. *J. Mol. Biol.*, **193**, 157–170.
24. Fourme, R., Kahn, R., Mezouar, M., Girard, E., Hörentrup, C., Prangé, T. and Ascone, I. (2001) High pressure protein crystallography (HPPX): instrumentation, methodology and results on lysozyme crystals. *J. Synchr. Rad.*, **8**, 1149–1156.
25. Colloc'h, N., Girard, E., Dhaussy, A.-C., Kahn, R., Ascone, I., Mezouar, M. and Fourme, R. (2006) High pressure macromolecular crystallography: the 140 MPa crystal structure at 2.3 Å resolution of urate oxidase, a 135-kDa tetrameric assembly. *Biochim. Biophys. Acta*, **1764**, 391–397.
26. Kennard, O., Cruse, W.B., Nachman, J., Prangé, T., Shakked, Z. and Rabinovitch, D. (1986) Ordered water structure in an A-DNA octamer at 1.7 Å resolution. *J. Biomol. Struct. Dyn.*, **3**, 623–647.
27. Watson, J.D. and Crick, F.H.C. (1953) A structure for deoxyribose nucleic acid. *Nature*, **171**, 737–738.
28. Doucet, J., Benoit, J.P., Cruse, W.B.T., Prangé, T. and Kennard, O. (1989) Coexistence of A- and B-form DNA in a single crystal lattice. *Nature*, **337**, 190–193.
29. Girard, E., Dhaussy, B., Couzinet, A.-C., Chervin, J.-C., Mezouar, M., Kahn, R., Ascone, I. and Fourme, R. Toward fully-fledged high pressure macromolecular crystallography (HPMX). *J. Appl. Cryst.*, in press.
30. Kabsch, W. (1993) Automatic processing of rotation diffraction data from crystals of initially unknown symmetry and cell constants. *J. Appl. Cryst.*, **26**, 795–800.
31. Collaborative Computational Program n°4 (CCP4) (1994) *Acta Crystallogr. D*, **50**, R760–763.
32. Shakked, Z., Rabinovitch, D., Kennard, O., Cruse, W.B., Salisbury, S.A. and Viswamitra, M.A. (1983) Sequence-dependent conformation of an A-DNA double helix. The crystal structure of the octamer d(G-G-T-A-T-A-C-C). *J. Mol. Biol.*, **166**, 183–201.

33. Navaza, J. (1994) AMoRe: an automated package for molecular replacement. *Acta Crystallogr. A*, **50**, 157–163.
34. Sheldrick, G.M. and Schneider, T.R. (1997) SHELXL: high resolution refinement. *Methods Enzymol.*, **277**, 319–343.
35. Dickerson, R.E. (1993) Program NEWHEL93, Molecular Biology Institute, Los Angeles, CA 90024, USA.
36. Kharakoz, D.P. and Sarvazyan, A.P. (1993) Hydrational and intrinsic compressibilities of globular proteins. *Biopolymers*, **33**, 11–26.
37. Teeter, M.M. and Hope, H. (1986) Expression, purification and characterization of recombinant crambin. *Trans. NY Acad. Sci.*, **482**, 163–165.